LLNL-PROC-736350
20th Biennial APS/Shock Compression Condensed Matter, St Louis MO, July 9-14, 2017

# VISAR fringe analysis under extreme spatially varying conditions

David J. Erskine[1,a)] and Dayne E. Fratanduono[1]

[1]*L-487, Lawrence Livermore Nat. Lab., Livermore, CA 94550, USA*

[a)]Corresponding author: erskine1@llnl.gov

**Abstract.** Many VISAR velocity interferometers employ a streak camera to record fringes along the spatial axis (Y) of a target, versus time. When the shock loading or target material property varies rapidly as a function of spatial position, the fringe phase (target velocity) varies rapidly versus Y. This challenges traditional algorithms since the apparent Y-spacing of fringes after the shock can be significantly different than the pre-shock (bias) spacing. For traditional column-by-column analysis the intensity signal would be a sinusoid with rapidly changing frequency, which can confuse a traditional algorithm, adding fluctuations in illumination caused by speckle. We describe a row-by-row approach to analyze such data called SPARVA (spatially resolving velocimetry analysis). Using a "sub-wave" configuration we are able to increase the spatial resolution by 3x, compared to conventional techniques.
August 29, 2017

## Introduction

The velocity interferometer system for any reflector (VISAR)[1, 2] is an important diagnostic for shock physics and equation of state (EOS) experiments, that measures the time history of Doppler shifted light reflected from shock or ramp loaded targets. Various algorithms for converting streak camera interferogram fringes to phase versus time signal are popular, including an FFT method[3], a sine fit along a column, and push-pull treatment of four rows at 90°[2, 4]. References 5, 6, 7 review several techniques. More recent algorithms using a row-by-row approach have been developed[8, 9], useful for removing ghost artifacts caused by unwanted reflection from stationary windows, due to the Lissajous style of data presentation[10, 11], and useful for illumination spatial variation.

We describe an improved version optimized for high-spatial resolution along the slit direction of the interferogram, called SPARVA for spatially resolving velocimetry analysis. This is useful for Y-variation caused by illumination speckle (Fig. 1a), shock arrival time variation (Fig. 1b, or Fig. 6) due to shock loading nonuniformity, or target material (granularity).

Generically, there can be two styles of analysis, by columns, or by rows (Fig. 2). The popular column by column

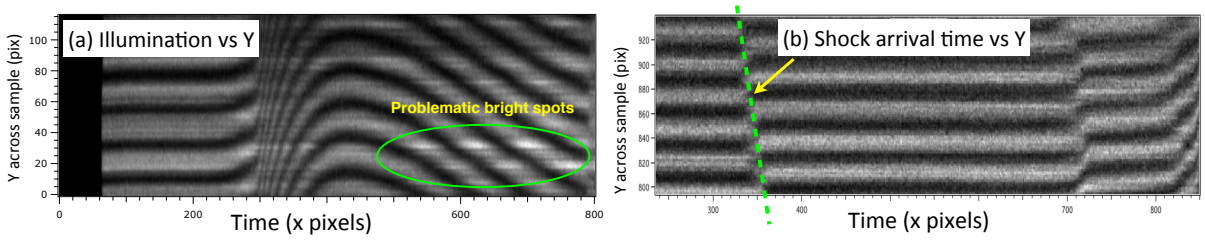


**FIGURE 1.** (a) Fluctuations in the illumination along the slit direction (Y), such as caused by laser speckle, produce artifacts in the normal analysis technique. (Omega shot s52238 by Ray Smith.) Each row has its gain adjusted to normalize the intensity. (b) Non-planar drive may produce "shearing" in the arrival time of events, whose accurate detection could be blurred by insufficient spatial resolution (NIF shot N110524).

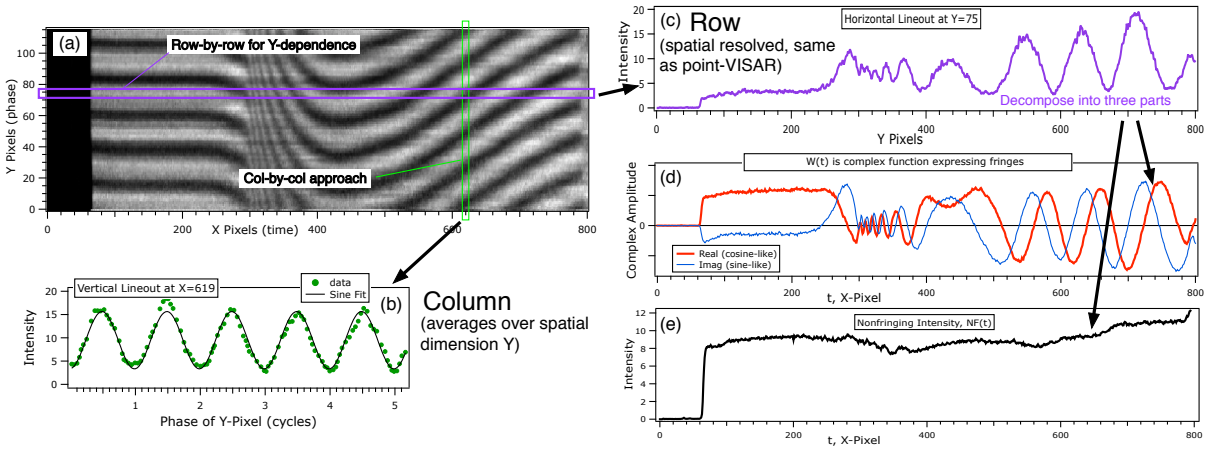


**FIGURE 2.** Two styles of analysis for a line VISAR interferogram (a), column-by-column (b) and row-by-row (c). In column-by-column an intensity lineout along the slit (Y axis) is fitted to a sinusoid, or a Fourier transform is performed. The phase of the sinusoid is proportional to target velocity. However this spatial averages over one or more Y-cycles (fringes). In a row-by-row method a set of four rows are combined arithmetically to yield real (red, cosine-like) and imaginary (blue, sine-like) parts (d), and nonfringing intensity (e)[2, 4]. Arctangent of real and imaginary parts yields time dependent phase. A better spatial resolution can be obtained in the row-by-row approach.

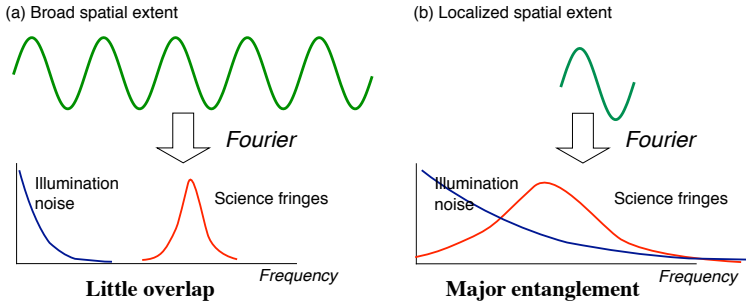


**FIGURE 3.** Column analysis issues. The reciprocal relation between spatial extent in Y and frequency extent causes the breadth of the peaks in Fourier space to broaden when the spatial extent is narrowed. This is a problem when the spatial extent is less than one fringe, because it increases the entanglement between the science peak and the (noisy) illumination peak.

Fourier method can be ill-suited for high spatial resolution, due to the uncertainty principle and use of fringes splayed along Y (Fig. 3). We optimized a row by row method to be robust to phase step changes, initially for a single fringe along Y ("full-wave), but discover that it also produces good results for spatial resolution *finer* than one fringe along Y ("sub-wave"). We have tested it on real and synthetic data.

## Method

The idealized "full-wave" push-pull method (Fig. 4[a]) measures intensity, $S_n$, in four row phases with 90° separation to produce a complex output $\mathbf{W}$ which holds the science,

$$2\mathbf{W} = (S_0 - S_2) + i(S_1 - S_3); \quad NF = (S_0 + S_1 + S_2 + S_3)/4 \tag{1}$$

and a nonfringing output $NF$ useful to monitor. The target velocity is proportional to the science phase $\theta$ (in units of cycles), which is found by the arctangent of the complex result $\tan 2\pi\theta = \Im\mathbf{W}/\Re\mathbf{W}$.

We find that it is possible to use <90° phase interval ("sub-wave", Fig. 4[b]). Adjustable weights $k_n$ are introduced

$$NF = (k_0 S_0 + k_1 S_1 + k_2 S_2 + k_3 S_3)/4. \tag{2}$$

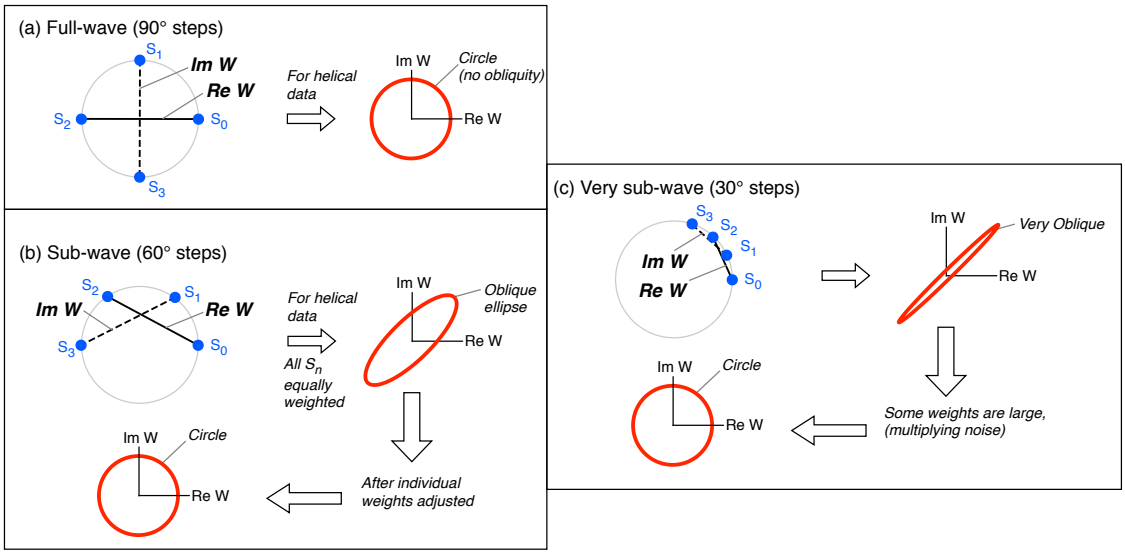


**FIGURE 4.** Example of full-wave (a), moderate sub-wave (b) and very sub-wave (c) phase step configurations. In the push-pull two difference are computed, $(S_0 - S_2)$ and $(S_1 - S_3)$ and assigned to real and imag parts of the complex output **W**. (a) Traditional "full wave" has four rows at 90°, which yields the ideal circular Lissajous. When the phase step is reduced (b)(c) producing a "sub-wave" configurations, an elliptical Lissajous results. This can be corrected by an "obliquity" operation, which magnifies the minor width relative to the major width. While this means some random noise is also magnified, it can improve the fidelity of measuring spatially varying phenomenon.

The $k_n$ are computed from geometry using intervals between row phases $\phi_n$, to produce a vector cancellation of fringes. (The $\phi_n$ of each $S_n$ can be estimated using the projection method, Eqs. 2-8 of Ref. 9). Negative $k_n$ are allowed to achieve cancellation, such as in the very sub-wave configuration where the average position of the $S_n$ is on one side of the circle. The nonfringing intensity is subtracted from each raw intensity, $S \leftarrow (S - NF)$, to produce a fringe-only version of $S_n$. Note that because pair differences are used in **W**, such as $(S_0 - S_2)$, errors in $NF$ cancel and do not affect **W**. However, an accurate $NF$ is beneficial to linearize the |**W**| vs $NF$ plot, described later.

For non-quadrature phase steps the Lissajous will initially be noncircular. The Lissajous is circularized by adjusting the data by an obliquity gain $g_q$, an astigmatic gain $g_{hv}$, and translational offsets $h_0$, $v_0$ (which also correct any ghost reflection artifact),

$$S'_0 = g_{hv}(S_0 + h_0); \quad S'_2 = g_{hv} S_2 \tag{3}$$

$$S'_1 = S_1 + v_0; \quad S'_3 = S_3. \tag{4}$$

The $S'_n$ are used for $S_n$ in Eq. 1 to recompute **W**. This is then modified by the obliquity operation

$$u = g_q(\Re W + \Im W); \quad v = \Re W - \Im W \tag{5}$$

$$\Re W' = (u + v)/2; \quad \Im W' = (u - v)/2 \tag{6}$$

$$W = \Re W' + i\,\Im W' \tag{7}$$

controlled by $g_q$, nominally unity, which magnifies the minor axis of the Lissajous ellipse relative to the major axis (see Eqs. 8-11 of Ref. 8). A test for judging Lissajous circularity is the linearity of magnitude |**W**| with nonfringing intensity $NF$ (Fig. 5[b]). The |**W**| vs $NF$ plot is only linear when every type of distortion is absent.

## Results

Figure 6 shows a test on NIF data which has mild Y-dependence of the post-shock velocity (phase), perhaps due to nonplanar loading. Figures 8 and 7 show a test on synthetic data which has a severe case of Y-dependence to the post-shock velocity (phase), and arrival time of shock. The Y-dependence is so strong that the apparent spacing of the fringe

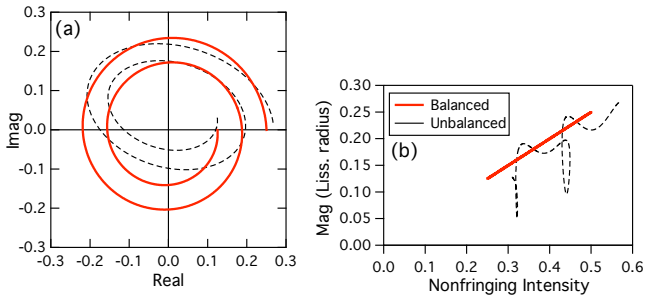


**FIGURE 5.** The magnitude |**W**| versus nonfringing intensity *NF* plot (b) is a key litmus test for judging centration. (a) Lissajous of ideal fringing data **W**(*t*) is centered (red curve), compared to non-ideal data (dashed) that is distorted. In the |**W**| versus *NF* plot (b) ideal data forms a line (red) and distortions cause nonlinear shapes (dashed). Reproduced from Ref. 8, copyright 2012 American Institute of Physics.

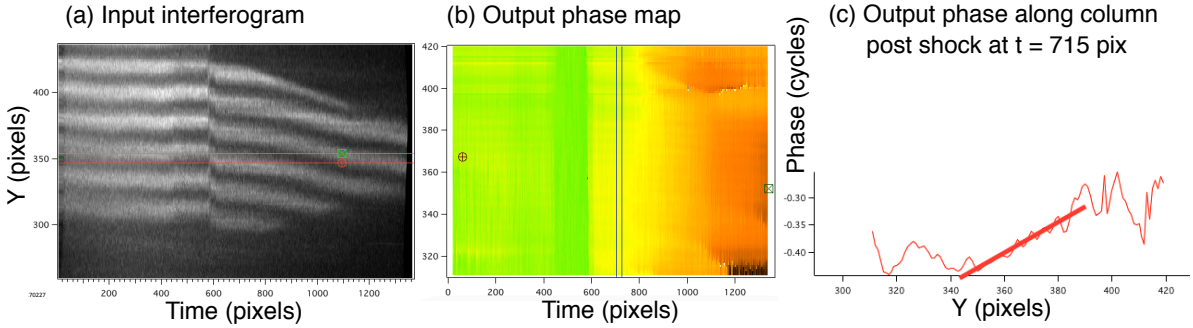


**FIGURE 6.** (a) Example interferogram where the phase of the post-shock fringe (after x > 600 pixel) varies versus Y about 0.1 cycle across target, perhaps due to uneven shock loading. (NIF shot N170227 taken by Amy Lazicki.) (b) The 2D phase map by our algorithm, after bias phase tilt removed. (c) Column lineout of the latter post-shock at t = 715 pixels showing a phase gradient.

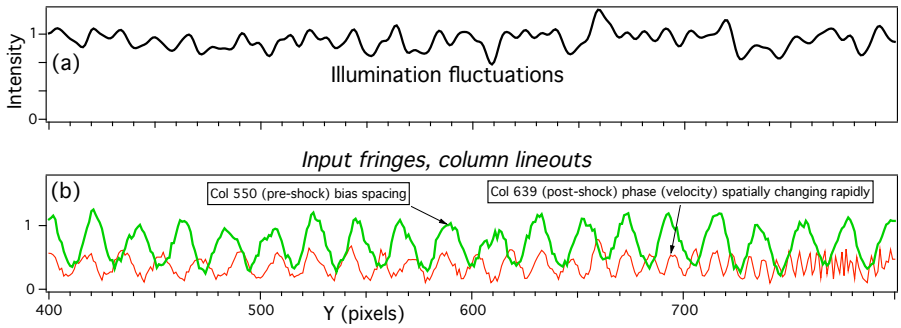


**FIGURE 7.** In creating the synthetic data of Fig. 8 we used illumination spatial fluctuations shown in (a) having energy in a variety of frequencies including that of the bias fringe frequency. Example column lineouts at X=550 prior to the shock (green), and X=639 post shock (red) show the effect of the fluctuations. Note that the apparent period of the fringe post shock is for Y> 600 significantly different than the quiescent bias period of 21 pixels. This is because we chose the shocked velocity to be a strong function of Y, and the apparent period is the rate of change of phase versus Y. Horizontal axis is Y in pixels along the slit direction.

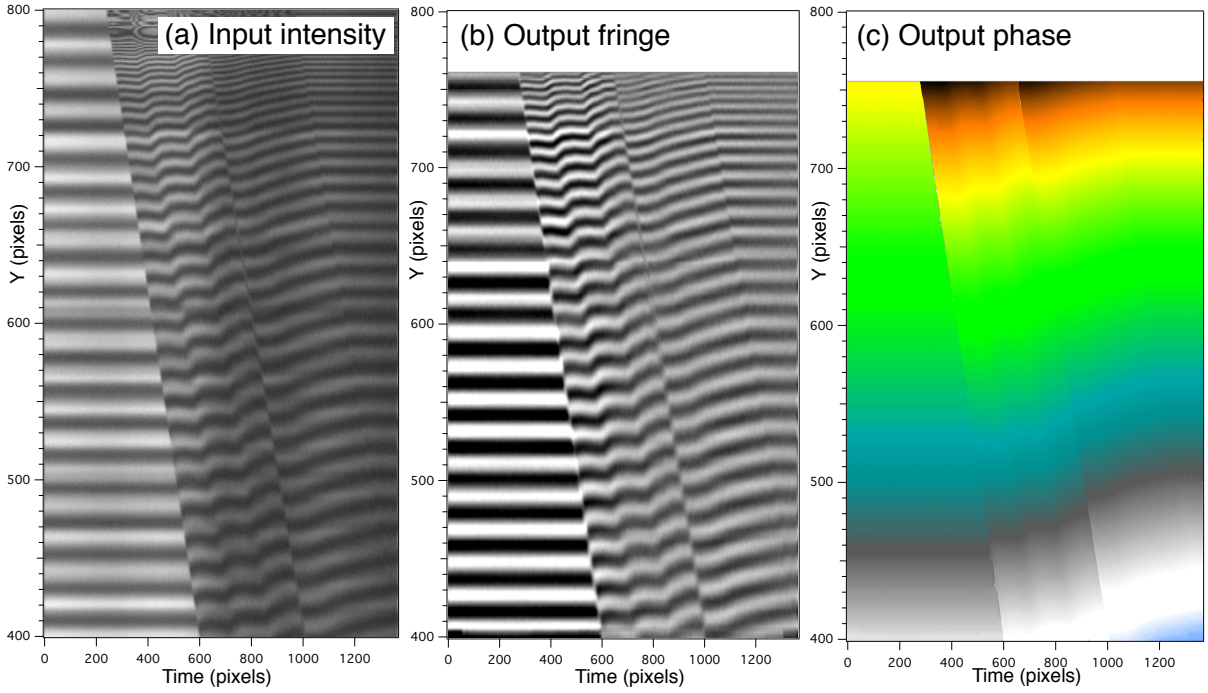


**FIGURE 8.** (a) Input interferogram. (b) Processed fringing component (real part), which is an intermediate output of the algorithm. (c) The outputted phase 2D map is the arctangent of the Lissajous. For Y below 640 the five sampled rows had a span of 21 pixels. For Y between 640 and 750 a smaller "sub-wave" span of 8 pixels was used, and above 750 a very small span of 6 pixels was used.

post-shock (red, Fig. 7b) is significantly smaller than the quiescent (bias) pre-shock value (green, Fig. 7b). Random fluctuations in the simulated illumination intensity (Fig. 7a) were used having a frequency range that included the bias fringe frequency. Hence one could not simply filter away the illumination noise since it occupies the same frequency range as the science. This challenging synthetic data was accurately processed by our algorithm.

Smaller phase steps demand more severe obliquity correction (Fig. 4[c]), which can magnify noise. The benefit of greater spatial resolution may reduce some error types in a tradeoff with increased other noise, such as detector noise. The nature of this tradeoff is under exploration but we suspect there is a minimum in total noise that encourages use of sub-wave phase steps, especially when the detector noise does not dominate.

We have found it beneficial to include a 5th row, $S_4$, that is four phase intervals away from $S_0$, averaging and substituting it as the first row $S_0 \leftarrow (S_0 + S_4)/2$. This significantly improves the robustness to changes in phase step, as shown by Hariharan (see page 210 of Ref. 12). An example apparent phase step change is along the time axis of our synthetic data, pre-shock compared to post-shock, due to spatially changing shock velocity (red to green curves in Fig. 7b). The 5th row also makes the Lissajous less oblique, which reduces noise magnification.

## ACKNOWLEDGMENTS

Thanks to Amy Lazicki and Ray Smith for Omega and NIF data. Prepared by LLNL under Contract DE-AC52-07NA27344.

## REFERENCES

[1] L. Barker and K. Schuler, "Correction to the Velocity-per-fringe Relationship for the VISAR Interferometer," *J. Appl. Phys.* **45**, 3692–3693 (1974).

[2] W. Hemsing, "Velocity Sensing Interferometer (VISAR) Modification," *Rev. Sci. Instr.* **50**, 73–78 (1979).

[3] M. Takeda, H. Ina, and S. Kobayashi, "Fourier-transform method of fringe-pattern analysis for computer-based topography and interferometry," *Journal of the Optical Society of America (1917-1983)* **72**, 156 (1982).

[4] W. M. Trott, M. D. Knudson, L. C. Chhabildas, and J. R. Asay, "Measurements of spatially resolved velocity variations in shock compressed heterogeneous materials using a line-imaging velocity interferometer," in *American Institute of Physics Conference Series*, *American Institute of Physics Conference Series* **505**, 993–998 (2000).

[5] P. M. Celliers, D. K. Bradley, G. W. Collins, D. G. Hicks, T. R. Boehly, and W. J. Armstrong, "Line-imaging velocimeter for shock diagnostics at the OMEGA laser facility," *Review of Scientific Instruments* **75**, 4916–4929 (2004).

[6] D. Dolan, "Foundations of VISAR analysis," *Sandia National Laboratory Tech. Rep.* **SAND2006-1950** (2006).

[7] M. K. Philpott, A. George, G. Whiteman, J. De'Ath, and J. C. F. Millett, "The application of line imaging velocimetry to provide high resolution spatially resolved velocity data in plate impact experiments," *Measurement Science and Technology* **26**, 125204 (2015).

[8] D. J. Erskine, R. F. Smith, C. A. Bolme, P. M. Celliers, and G. W. Collins, "Two-dimensional imaging velocity interferometry: Data analysis techniques," *Review of Scientific Instruments* **83**(4), 043116 (2012).

[9] D. Erskine, "Speckle-adaptive VISAR fringe analysis technique," in *19th Biennial APS Conference on Shock Compression of Condensed Matter*, *American Institute of Physics Conference Series* **1793**, 160017 (2017).

[10] D. Erskine, J. Eggert, P. Celliers, and D. Hicks, "Ghost fringe removal techniques using Lissajous data presentation," in *19th Biennial APS Conference on Shock Compression of Condensed Matter*, *American Institute of Physics Conference Series* **1793**, 160016 (2017).

[11] D. J. Erskine, J. H. Eggert, P. M. Celliers, and D. G. Hicks, "Ghost fringe removal techniques using Lissajous data presentation," *Review of Scientific Instruments* **87**, 033106 (2016).

[12] P. Hariharan, *Basics of Interferometry, Second Ed.*, Academic Press, an imprint of Elsevier, London, UK (2007).